

Phonon anomalies in β -phase $\text{Ni}_x\text{Al}_{1-x}$ alloys

G. L. Zhao and B. N. Harmon

Ames Laboratory, and Department of Physics, Iowa State University, Ames, Iowa 50011-3010

(Received 21 February 1991; revised manuscript received 21 August 1991)

The electronic band structure of β -phase $\text{Ni}_x\text{Al}_{1-x}$ has been calculated using a first-principles linear combination of atomic orbitals method, and then fitted by the nonorthogonal empirical tight-binding method for the evaluation of electron-phonon matrix elements. A Kohn-like anomaly in the TA_2 branch along the $[110]$ direction is attributed to both strong electron-phonon interactions and Fermi-surface nesting. Other phonon anomalies near $\mathbf{q}=0.55(1,1,1)\pi/a$ and $\mathbf{q}=0.6(1,0,0)\pi/a$ in β -phase $\text{Ni}_{0.50}\text{Al}_{0.50}$ are predicted. For the $\text{Ni}_{0.625}\text{Al}_{0.375}$ composition, the TA_2 anomaly shifts to smaller wave vectors and the phonon is predicted to be soft at $T=0$ K. Introducing a thermal smearing of the Fermi surface is enough to stabilize this mode, which occurs near $(\frac{1}{3}, \frac{1}{3}, 0)\pi/a$ and is associated with the well-known martensitic transformation.

I. INTRODUCTION

Martensitic transformations have been perplexing scientists for over a century. It was only with the discovery and application of x-ray diffraction to steels, that the fundamental nature of such transformations was established.¹ They involve the cooperative, rather than diffusive, displacement of atoms. The size of the displacements can be a large percentage of the lattice constant, and the resulting crystal symmetry is altered. Displacive transformations occur in a wide variety of materials and are further classified from weak (almost second order) to strongly first order.² Among those materials which exhibit transformations intermediate between these extremes, β -phase $\text{Ni}_x\text{Al}_{1-x}$ alloys are the prototypical examples and have received extensive study by neutron, x-ray, and electron scattering, as well as numerous other techniques. Many of these studies are quite recent, and have provided a wealth of details concerning the transformation.³ There is also a growing optimism that a complete microscopic analysis of such transformations will soon be within reach.³ In this paper we focus on the phonon structure of Ni-Al alloys and relate it to the underlying electronic structure, an important ingredient in the "mechanics" of many martensitic transformations.

The cesium chloride or β -phase structure of $\text{Ni}_x\text{Al}_{1-x}$ alloys is well known for exhibiting a martensitic phase transformation for x near 0.62.⁴⁻¹² In the high-temperature phase, neutron scattering measurements have revealed phonon anomalies that strengthen as the temperature is lowered toward the transformation temperature, T_M . The anomalies are also dependent on the concentration x and the applied stress; and occur at those phonon wave vectors related to the transformation displacements.¹¹⁻¹³ Among investigators studying such phenomena there is the belief that "the phonons are the roadmaps" for the physics of the transformations.¹⁴ Indeed, the large decrease in vibrational frequency observed as the temperature is lowered is quite anomalous

and is indicative of strong anharmonic interactions. In the last few years it has been realized that these anharmonic forces are the key to understanding many martensitic transformations.^{5,15-21} In this paper we concentrate on the phonons themselves, rather than on the large displacements occurring for the transformations. We are able to identify a nesting feature of the Fermi surface as the electronic origin of the phonon anomaly and to trace its dependence on concentration. Other recent studies relate the anomalies to anharmonic forces for large displacements,⁵ and to the observed pseudoelastic behavior under applied stress.¹⁶

The electronic structure of NiAl has been the subject of numerous investigations.²²⁻³⁰ In general there is good agreement among the theoretical band structure calculations. (See Ref. 22 for a comparison of several theoretical studies along with detailed data from angle resolved photoemission experiments. Reference 23 gives a comparison between theory and experiment for the optical conductivity up to ~ 6 eV.) The electronic structure of ordered NiAl is of course easily evaluated using modern band structure methods, while the consideration of concentration changes (x dependence) or disorder requires further approximations which we address later.

The experimental determination of the bulk and surface vibrational modes of NiAl have recently been reported,³¹ and we first concentrate on the theoretical determination of these phonon dispersion curves (for the bulk $x=0.5$ alloy). We then follow the weak anomaly in the transverse $[110]$ branch and show how it moves and strengthens as x approaches the values where the martensitic transformation occurs. The transformation temperature, T_M , is also very sensitive to the concentration and varies from 0 K to 400 K as x varies from 0.60 to 0.68.⁹⁻¹² While we are unable to accurately treat the temperature dependence, we do show how a thermal smearing of the sharp Fermi-surface nesting feature affects the phonon anomaly in a manner consistent with the experiments.

II. ELECTRONIC STRUCTURE AND THE PHONON SPECTRUM OF β -PHASE NiAl

A. Method

We have used a self-consistent first-principles linear combination of atomic orbitals (LCAO) method³² to calculate the electronic band structure of NiAl . The same method was also used in our study of the electron-phonon interactions in NiTi .³³ In this method the s , p , and d radial functions are expanded in a series of 18, 18, and 15 Gaussian functions, respectively, and the required integrals performed analytically. The method is quite accurate and our results for the energy bands and density of states are very similar to previous first-principles studies.^{22,23} In order to calculate the electron-phonon (e -ph) interaction matrix elements for use with the method of Varma and Weber,³⁴ the first-principles band structure was fitted using a nonorthogonal Slater-Koster tight-binding (TB) Hamiltonian. The empirical TB model included s , p , and d states on Ni, and s and p states on Al. Thirteen bands of 15 high-symmetry \mathbf{k} points have been fitted. When the energy bands around the Fermi energy, ($E_F=0$), are given higher weight, the overall RMS error is about 1.8 mRy, with the fit errors for the energy bands around E_F being about 1 mRy. The TB energy bands are shown in Fig. 1. From Fig. 1 it can be seen that only the energy bands 6 and 7, counted from the bottom, cross the Fermi energy. These are the bands which will be included in the calculation of the e -ph interaction. The TB bands around the Fermi energy differ insignificantly from the first-principles results. High quality TB bands are vital for the calculation of the e -ph interaction, since a subtle distortion of the Fermi surface may smear out any nesting feature contributing to the phonon anomaly. The total and partial electron density of states (DOS) are given in Fig. 2. One interesting feature of the DOS is that there is a sharp dip in the Ni d states at -0.058 Ry, which almost divides the d -electron states of nickel into

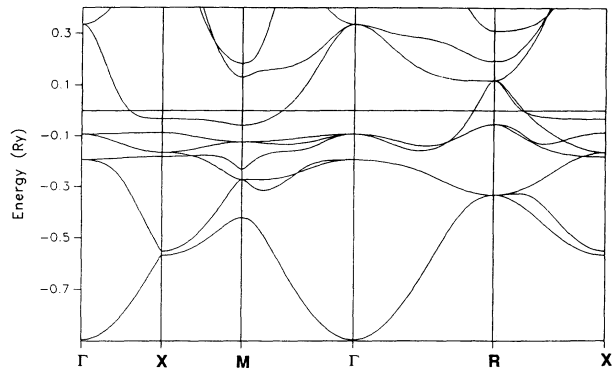


FIG. 1. The electronic energy bands of β -phase NiAl . The bands were calculated by using a first-principles LCAO method and then fitted by using an empirical tight-binding Hamiltonian.

two parts. Only the antibonding d states of Ni which mix with the s and p states of Al are located near the Fermi energy. The four low energy d bands of Ni are full and it is found that the total d occupation is close to 9.0, the same as for pure Ni.

To proceed with the evaluation of the electron phonon coupling we follow Varma and Weber³⁴ and write the dynamical matrix as

$$D = D_0 + D_1 + D_2, \quad (1)$$

where ($D_0 + D_1$) are the short-range interactions between the atoms, which will be depicted by a Born-von Kármán force constant model; D_2 is the contribution from the e -ph interaction, which is given by³⁵

$$D_2(\kappa\alpha, \kappa'\beta | \mathbf{q}) = - \sum_{\mathbf{k}, \mu, \nu} \frac{f_{\mathbf{k}\mu}(1 - f_{\mathbf{k}+\mathbf{q}, \nu})}{\varepsilon_{\mathbf{k}+\mathbf{q}, \nu} - \varepsilon_{\mathbf{k}\mu}} g_{\mathbf{k}, \mu; \mathbf{k}+\mathbf{q}, \nu}^{\kappa\alpha} g_{\mathbf{k}+\mathbf{q}, \nu; \mathbf{k}, \mu}^{\kappa'\beta} \quad (2)$$

in which

$$g_{\mathbf{k}\mu, \mathbf{k}'\nu}^{\kappa\beta} = \sum_{\beta_1, m_1, \beta_2, m_2} A^*(\mathbf{k}'\nu | \beta_1 m_1) [\gamma_\alpha(\beta_1 m_1 \beta_2 m_2 | \mathbf{k}) \delta_{\beta, \beta'} - \gamma_\alpha(\beta_1 m_1 \beta_2 m_2 | \mathbf{k}') \delta_{\beta_2, \beta}] A(\mathbf{k}\mu | \beta_2 m_2) \quad (3)$$

and

$$\gamma_\alpha(\beta_1 m_1 \beta_2 m_2 | \mathbf{k}) = \sum_l \langle \phi_{\beta_1 m_1} | \frac{\partial H}{\partial u_\alpha(\beta_1 l_1, \beta_2 l_2)} | \phi_{\beta_2 m_2} \rangle \times e^{-i\mathbf{k} \cdot \mathbf{R}(\beta_1 l_1, \beta_2 l_2)}. \quad (4)$$

Here $|\phi_{\beta m}\rangle$ is the m th orbital of the atomic wave function of site β ; $\mathbf{R}(l_1 \beta_1, l_2 \beta_2) = \mathbf{R}(l_1 \beta_1) - \mathbf{R}(l_2 \beta_2)$; $A(\mathbf{k}\mu | \beta m)$ is the (βm) component of μ th eigenstate at the point \mathbf{k} . $\varepsilon_{\mathbf{k}\mu}$ is the energy of the μ th band at \mathbf{k} ; $f_{\mathbf{k}\mu}$ is the Fermi distribution function; H is the Hamiltonian; and $u_\alpha(\beta l)$ is the displacement of the atom at the β site of the l th cell.

In our calculation the Brillouin zone was partitioned

into cubes on a $\pi/(20a)$ mesh. In the standard $\frac{1}{48}$ th region of the Brillouin zone, there are 1771 \mathbf{k} points on a mesh of cube corners which will be used to calculate the energy, $E(\mathbf{k})$. There are 1540 \mathbf{k} points, which are located in the centers of the cubes and the wave functions at these \mathbf{k} points are used to calculate the e -ph matrix elements which are assumed constant within each small cube. The actual Brillouin zone sum depends on the symmetry of the phonon wave vector and use is made of group theory to keep the calculation manageable.

B. Results

The phonon dispersion curves of a β -phase NiAl single crystal with the stoichiometry 0.506 ± 0.002 Al have been

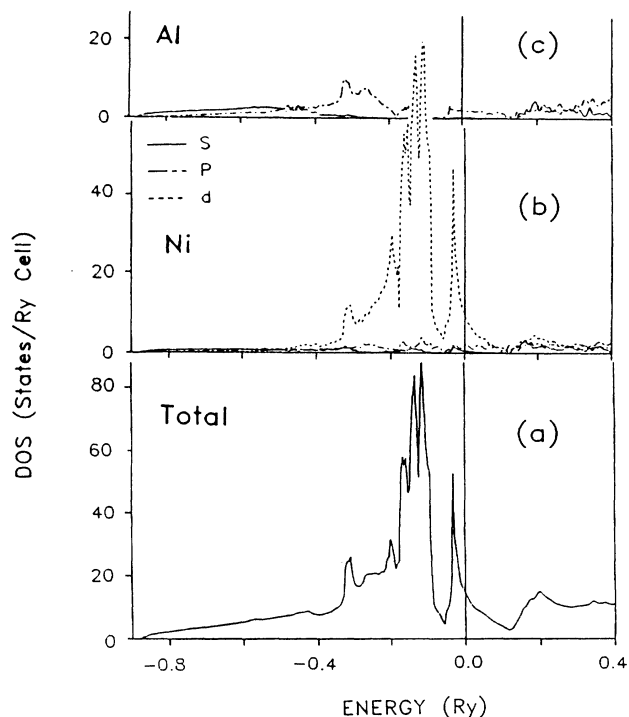


FIG. 2. The total and partial electronic density of states of β -phase NiAl.

recently measured by neutron scattering.³¹ A weak phonon anomaly was found in the lower transverse branch along the [110] direction, which could not be reproduced by fitting the results with Born-von Kármán force models extending to third- and fourth-nearest neighbors.³¹

We have used the Born-von Kármán model to represent the contribution of $(D_0 + D_1)$ to the dynamical matrix. We used axially symmetric force constants and included interactions to the second shell for each atomic pair (Ni-Ni, Ni-Al, and Al-Al pairs) to fit the measured phonons. The force constants for $(D_0 + D_1)$ are listed in Table I. Without including the e -ph interaction (D_2) but using the axially symmetric model, the fitted average RMS error can be optimized to 0.19 THz and the calculated results are almost identical to those of Ref. 31. The phonon anomaly in the transverse branch along [110] direction cannot be reproduced. When the e -ph interactions were evaluated and included in the phonon dynamical matrix D_2 , the calculated phonon dispersion curve displayed the phonon anomaly in the $TA_2[110]$ branch, as shown in Fig. 3(a). There is an inconsistency in the literature in labeling this branch. We follow Refs. 4, 9, and 13 in labeling it TA_2 . It has a polarization vector along the $[1\bar{1}0]$ direction. Phonon dispersion curves along the [111] and [100] directions are also given in Figs. 3(b) and 3(c). The average RMS difference between the calculated phonon frequencies and the measurement is about 0.15 THz.

The most prominent phonon anomaly of β -phase NiAl is the broad and shallow dip along the [110] direction, which is stable even at low temperature. This is consistent with the experimental finding that the β -phase

$Ni_{0.50}Al_{0.50}$ alloy is stable and does not transform to another phase at low temperature.^{11,12} It is different from the phonon anomaly of the β -phase of NiTi, which exhibits a sharp phonon dip and a completely soft phonon at low temperatures.^{33,36,37}

We have also performed the calculations by evaluating the Fermi distribution function in Eq. (2) at temperatures of 1, 296, and 500 K. The higher temperature results in a

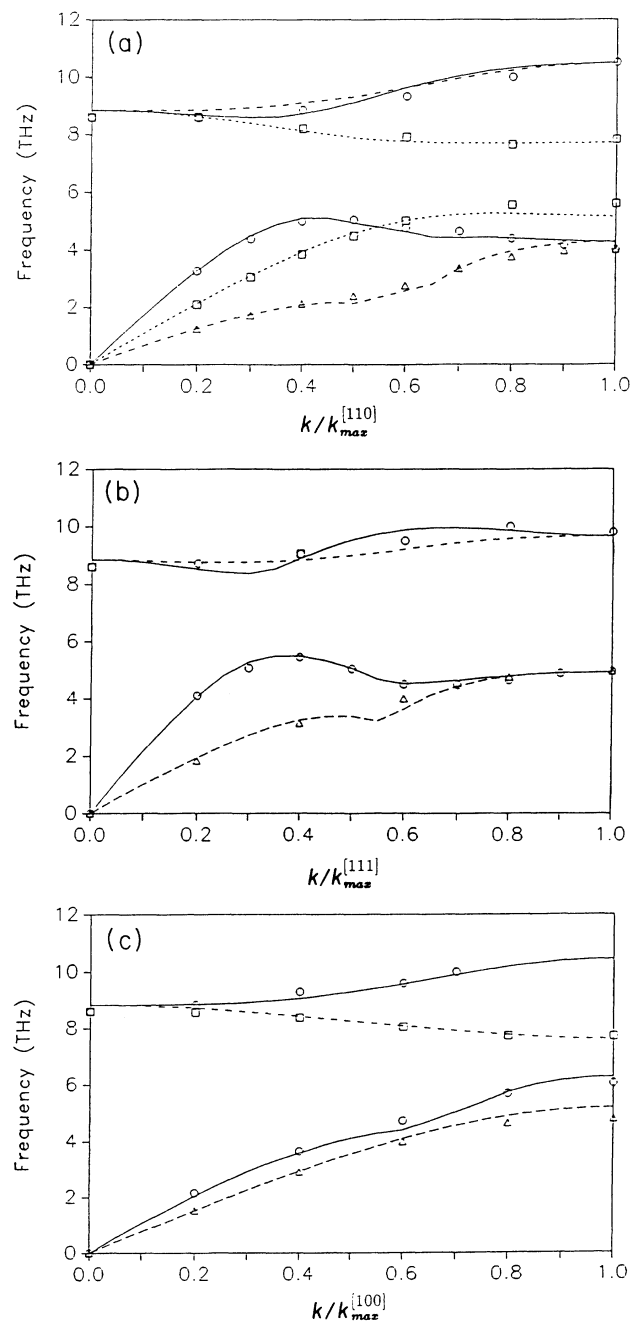


FIG. 3. The phonon dispersion curves of the β -phase NiAl, along the three directions, [110], [111], and [100]. All the lines are the calculated results and the symbols are the experimental results (Ref. 31). Solid lines and circles represent the longitudinal modes, dashed lines and triangles (or squares) the transverse modes.

TABLE I. The longitudinal (l) and transverse (t) short-range axially symmetric force constants for $(D_0 + D_1)$ used in the Born-von Kármán model for the β -phase of Ni-Al. The full dynamical matrix also includes the long-range electronic interaction given by Eqs. (1) and (2).

Pair	Coordination shell	r (Å)	(l) (10^3 dyn/cm)	(t) (10^3 dyn/cm)
Ni-Ni	1st	2.8864	6.8243	-1.3819
	2nd	4.0820	6.2983	-0.1671
Ni-Al	1st	2.4997	32.7441	0.0408
	2nd	4.7866	1.2782	0.1659
Al-Al	1st	2.8864	20.2224	-0.5254
	2nd	4.0820	3.0884	-0.4070

smearing of the Fermi surface, but does not account for the additional smearing caused by the static and dynamic disorder. The phonon frequency at the anomaly $\mathbf{q}=0.5(1,1,0)\pi/a$ is reduced from 2.23 THz at 500 K to 2.19 THz at 1 K. The change of the phonon frequency between these two temperatures is only about 1.8%. This is quite small and changes in phonon frequency due to other effects such as phonon-phonon interactions and lattice expansion may well be larger. Another interesting finding from the calculation is that the phonon dispersion curves of the β -phase NiAl will also have a phonon anomaly in the TA mode along the [111] direction around $0.55(1,1,1)\pi/a$ which should be measurable. Another weak phonon anomaly in the LA mode along the [100] direction near $0.6(1,0,0)\pi/a$ is also predicted, but may be too small and difficult to measure.

III. CALCULATIONS FOR β -PHASE $\text{Ni}_x\text{Al}_{1-x}$ ALLOYS

The $\text{Ni}_x\text{Al}_{1-x}$ alloys undergo a martensitic phase transformation for $0.60 < x < 0.68$ with the transition temperature varying between $10 \text{ K} < T_M < 400 \text{ K}$.^{11,12} A neutron scattering study found that the transverse acoustic phonon of $\text{Ni}_{0.625}\text{Al}_{0.375}$ along the $[\xi\xi 0]$ direction exhibited a marked, but incomplete softening at $\xi = \frac{1}{6}(2\pi/a)$, which was also temperature dependent. The position of this phonon anomaly along the [110] direction also depends on the composition, x . Increasing the Ni concentration, the position of the phonon anomaly shifts toward the zone center.¹¹ A calculation for $\text{Ni}_{0.625}\text{Al}_{0.375}$ is difficult because the excess nickel will randomly occupy Al sites and lead to some disorder, making accurate first-principles calculations infeasible at present. Even if the excess nickel atoms were ordered in a superlattice structure, first-principles calculations would be very difficult because of the need to consider very large unit cells. Instead we have used a rigid band model to trace the phonon anomaly and to offer some insight into the effects of compositional changes. Because the $\text{Ni}_x\text{Al}_{1-x}$ alloys used in the experiments were single crystals with the same CsCl crystal structure, we start with the same band structure, that of the β -phase $\text{Ni}_{0.50}\text{Al}_{0.50}$ alloy. The Fermi energies will be different for different compositions in these alloys since the number of valence electrons will depend on x .

A naive application of the rigid-band model would as-

sign 10 valence electrons to Ni and 3 to Al, and the excess Ni would then raise the Fermi level above that of the 50-50 alloy. This does not work for explaining the shifts in optical spectra as a function of concentration.²³ The 3d electrons are highly correlated, and first-principles calculations for other compounds containing Ni show that Ni maintains a d -electron occupation very close to 9.0—the same as for elemental Ni metal. It is therefore more appropriate to consider the d^9 configuration as fixed (corelike) so that each additional Ni atom only adds a single valence electron to the rigid bands of the 50-50 alloy. Thus the Fermi level is lowered as the Ni concentration increases. This is consistent with the optical spectra,²³ and gives a very reasonable explanation for the concentration dependence of the phonon anomaly, as we describe below. Very recent KKR-CPA calculations which do take into account the compositional disorder are in substantial agreement with this picture.³⁸

Using the rigid-band model as explained above, we have calculated the e -ph interaction for the β -phase $\text{Ni}_{0.625}\text{Al}_{0.375}$ by shifting the Fermi energy down 0.0218 Ry relative to that of the $\text{Ni}_{0.50}\text{Al}_{0.50}$ alloy. Actually this energy shift corresponds to $\text{Ni}_{0.60}\text{Al}_{0.40}$ if the d^9 constraint is strictly applied (the concentration dependence is discussed later). Keeping the same short-range force constants (Table I), the calculated phonons along the [110] direction are shown in Fig. 4. From Fig. 4, it is seen that the $\text{TA}_2[110]$ phonon has a very strong phonon anomaly

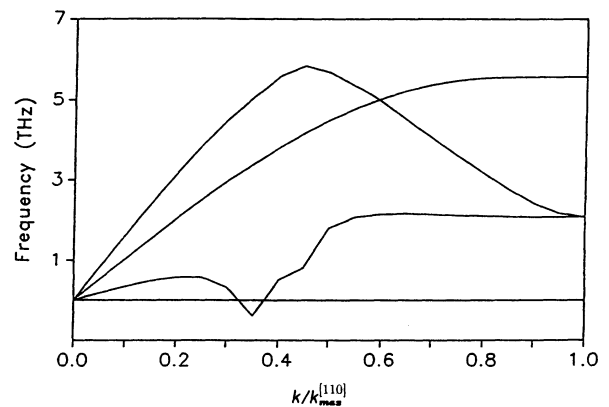


FIG. 4. Phonon dispersion curves calculated at $T=0 \text{ K}$ corresponding to the β -phase $\text{Ni}_{0.625}\text{Al}_{0.375}$ alloy.

and becomes completely soft near $\mathbf{q}=0.35(1,1,0)\pi/a$. The calculations were performed without regard for temperature effects and are strictly speaking only valid for $T=0$ K. Experimentally the dip in the TA_2 dispersion curve becomes deeper as the temperature is lowered, but the transformation takes place before the phonon frequency goes to zero. This is in contrast to the case of NiTi where there is a TA_2 phonon which does go soft before the actual martensitic transformation.^{36,37} In previous calculations we showed that this phonon anomaly in NiTi is also caused by Fermi-surface nesting and strong e -ph coupling.³³ The dramatic temperature dependence of these anomalies can be associated with the smearing of the nesting feature of the Fermi surface as T increases. The disorder in the $Ni_{0.625}Al_{0.375}$ alloy will have a similar effect as the temperature in smearing the Fermi surface, thus the completely soft phonon in Fig. 4 near $\mathbf{q}=0.35[1,1,0]\pi/a$, will be hardened by the combined effects of compositional disorder, thermal disorder (vibration of the atoms) and the thermal smearing of the Fermi surface. A direct calculation including these effects on the phonon frequency is extremely difficult. We have therefore used a temperature smearing of the Fermi distribution to simulate all the disorder contributions. In Fig. 5, a temperature of 1000 K has been used in the Fermi distribution function to compare the calculated results with the experimental measurement. The squares for the lower branch are the TA_2 phonons measured at room temperature, the triangles are the TA_1 modes, and the open circles are the longitudinal acoustic phonons. The solid lines correspond to the theory which shows that the TA_2 phonons become stable, and only a marked phonon

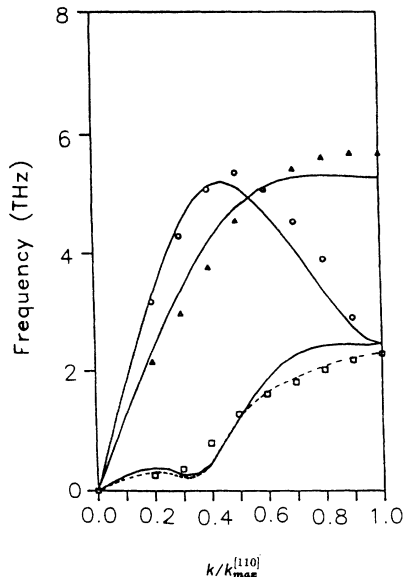


FIG. 5. Calculated phonon dispersion curves (solid lines) of the β -phase $Ni_{0.625}Al_{0.375}$ alloy for which a temperature of 1000 K has been used in the Fermi distribution function in order to simulate the effects of disorder in smearing the Fermi surface. The symbols are the experimental results at room temperature. Dashed line depicts the experimental results at $T=85$ K (Refs. 9 and 12).

anomaly persists. The dashed curve shows the TA_2 phonons measured at $T=85$ K,^{9,12} just above the martensitic transformation temperature. Note that we fit the (D_0+D_1) short-range force constants using all the phonons measured at room temperature.

IV. DISCUSSION AND CONCLUSIONS

The Fermi-surface nesting which is responsible for the $TA_2[110]$ phonon anomaly is shown in Fig. 6. The Fermi surface in Fig. 6 corresponds to same electron occupation as used for the calculation of Fig. 4. The figure shows the Fermi surface in k_x - k_y planes for three different values of k_z ($0.25\pi/a$, $0.38\pi/a$, and $0.48\pi/a$). One of the nesting regions is indicated by the arrow, and the others (related by symmetry) are obvious. In order for there to be a peak in the generalized susceptibility (and hence in D_2) the nesting shown in the $k_z=0.38\pi/a$ plane must extend some distance perpendicular to the plane. We find there is significant nesting extending between $k_z=0.25\pi/a$ and $k_z=0.48\pi/a$. The generalized susceptibility [Eq. (2) with no e -ph matrix elements] is frequently calculated as a useful function for identifying where in q -space phonon anomalies are likely to occur. For nesting the susceptibility exhibits a peak, and this is shown in Fig. 7. While the peak is not particularly dramatic (the volume in the k space that is actually "nested" is quite small), the peak together with very strong transverse mode e -ph matrix elements is enough to drive the already low frequency TA_2 phonons soft (at least for the theory at $T=0$ K). This is very similar to the situation we encountered for NiTi.³³

The β -phase Ni_xAl_{1-x} alloys for different concentration can be considered by shifting the Fermi energy in a rigid band fashion as we have described. The position of the anomaly, Q_{min} , of the TA_2 phonon along the $[110]$ direction for β -phase Ni_xAl_{1-x} alloys is given in Fig. 8.

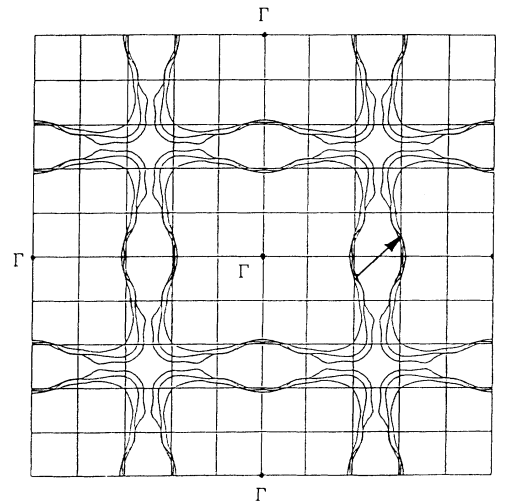


FIG. 6. The Fermi surface showing the nesting feature of the β -phase $Ni_{0.625}Al_{0.375}$ alloy. The k_x - k_y planes with three different values of k_z ($0.25\pi/a$, $0.38\pi/a$, and $0.48\pi/a$) are shown, and the arrow indicates two nested surfaces.

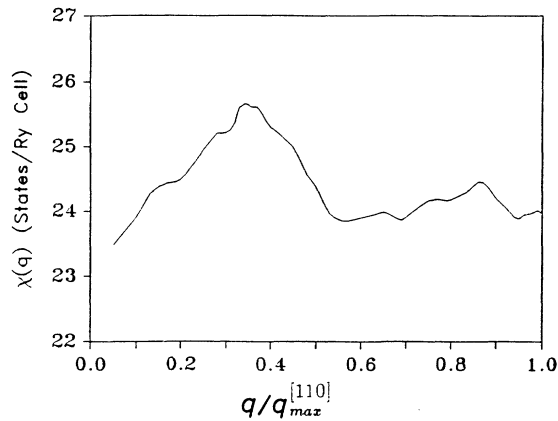


FIG. 7. Calculated results of the generalized susceptibility, $\chi(\mathbf{q})$, along the [110] direction, of the β -phase $\text{Ni}_{0.625}\text{Al}_{0.375}$ alloy. Note the large "background."

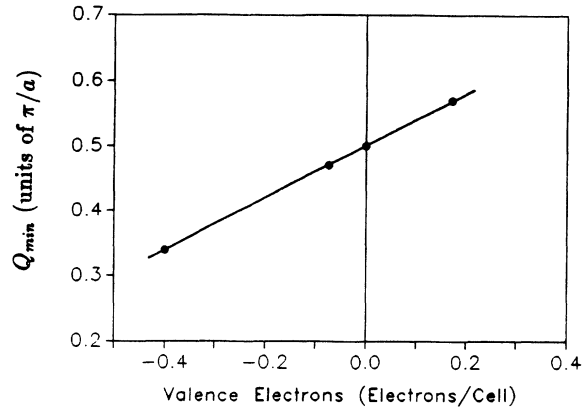


FIG. 8. The calculated positions of the phonon anomaly, Q_{\min} , along the [110] direction as the function of the number of valence electrons. (Zero corresponds to the β -phase $\text{Ni}_{0.50}\text{Al}_{0.50}$).

Here we determine the position of Q_{\min} by identifying it with the peak in the generalized susceptibility. The susceptibility can be calculated on a much finer q mesh if e - ph matrix elements are not required. We find that the calculated position of the phonon anomaly has a linear relation with the electron concentration as has been found in the neutron scattering.^{11,12} It should be noticed that the units of Q_{\min} in Fig. 8 are π/a instead of $2\pi/a$ which are used in reporting many experimental results. We also note that if the one electron per Ni atom constraint for the rigid-band model were strictly applied then the Ni 0.625 concentration would correspond to -0.5 valence electrons in Fig. 8 and the Q_{\min} would occur at $\approx 0.3\pi/a$.

We are somewhat limited in our analysis by having to assume a rigid-band model. However this model appears quite useful since a number of features of the observed phonon anomalies depend on the Fermi-surface nesting, the existence of which suggests a long-range coherence in the electronic structure. (As mentioned earlier, this has recently been confirmed by KKR-CPA calculations.³⁸) Since compositional and vibrational (thermal) disorder both act to smear the Fermi surface, we have been partially able to simulate these effects by using temperature as a parameter in the Fermi distribution function. As

Figs. 4 and 5 demonstrate, the smearing of the nesting is enough to stabilize the soft phonon. Since we perform our calculations on a $\pi/(20a)$ mesh we are unable to be extremely precise as to the position of the dip. The actual lock-in of the wave vector to $q_{7R} = (2/7, 2/7, 0)\pi/a$ involves higher-order terms in the energy vs displacement relation than we have considered. Finally we note that the possibility of compositional fluctuations in the β -phase $\text{Ni}_x\text{Al}_{1-x}$ alloys for $0.60 < x < 0.68$, could lead to variations in the degree of the disorder for different regions of the material. A region with less disorder could result in the anomalous phonon going completely soft. This region would then act as a nucleation center for the phase transformation. This is similar to the idea of "localized soft modes" as a response to defect strains.³⁹

ACKNOWLEDGMENTS

We are thankful to L. Tanner and S. Shapiro for several stimulating discussions. Ames Laboratory is operated for the U.S. Department of Energy by Iowa State University under Contrast No. W-7405-Eng-82. This work was supported by the Director for Energy Research, Office of Basic Energy Sciences of the U.S. Department of Energy.

¹For an historical account of E. C. Bain's early application of x rays to martensitic transformation, see H. W. Paxton and J. B. Austin, *Metall. Trans.* **3**, 1035 (1972).

²L. E. Tanner and M. Wuttig, *Mater. Sci. Eng.* **A127**, 137 (1990).

³The Proceedings of the Workshop on First-Order Displacive Phase Transformations, edited by L. E. Tanner and M. Wuttig [*Mater. Sci. Eng.* **A127**, 137 (1990)].

⁴Y. Noda, S. M. Shapiro, G. Shirane, Y. Yamada, and L. E. Tanner, *Phys. Rev. B* **42**, 10 397 (1990).

⁵Y. Yamada, Y. Noda, and K. Fuchizaki, *Phys. Rev. B* **42**, 10 405 (1990).

⁶Y. Yamada, *Metall. Trans.* **19A**, 777 (1988).

⁷V. S. Litvinov, L. P. Zelenin, and R. Sh. Shklyar, *Fiz. Metal. Metalloved.* **31**, 138 (1971).

⁸I. M. Robertson and C. M. Wayman, *Philos. Mag. A* **48**, 421 (1983).

⁹S. M. Shapiro, *Mat. Sci. Forum* **56-58**, 33 (1990).

¹⁰Y. K. Au and C. M. Wayman, *Scr. Metall.* **6**, 1209 (1972).

¹¹S. M. Shapiro, J. Z. Larese, Y. Noda, S. C. Moss, and L. E. Tanner, *Phys. Rev. Lett.* **57**, 3199 (1986).

¹²S. M. Shapiro, B. X. Yang, G. Shirane, Y. Noda, and L. E. Tanner, *Phys. Rev. Lett.* **62**, 1298 (1989).

¹³L. E. Tanner, D. Schryvers, and S. M. Shapiro, *Mater. Sci. Eng.* **A127**, 205 (1990).

¹⁴L. E. Tanner, private communication.

- ¹⁵K. M. Ho and B. N. Harmon, *Mater. Sci. Eng.* **A127**, 155 (1990).
- ¹⁶Y. Y. Ye, C. T. Chan, and K. M. Ho, *Phys. Rev. Lett.* **66**, 2018 (1991).
- ¹⁷R. J. Gooding, *Mater. Sci. Eng.* **A127**, 183 (1990).
- ¹⁸J. A. Krumhansl, in *Nonlinearity in Condensed Matter*, edited by A. R. Bishop, D. K. Campbell, P. Kumar, and S. E. Trullinger (Springer-Verlag, Berlin, 1986), p. 255.
- ¹⁹J. A. Krumhansl and Y. Yamada, *Mater. Sci. Eng.* **A127**, 167 (1990).
- ²⁰K. Enami, J. Hasunuma, A. Nagasawa, and S. Nenno, *Scr. Metall.* **10**, 879 (1976).
- ²¹R. J. Gooding and J. A. Krumhansl, *Phys. Rev. B* **39**, 1535 (1989).
- ²²S. C. Lui, J. W. Davenport, E. W. Plummer, D. M. Zehner, and G. W. Fernando, *Phys. Rev. B* **42**, 1582 (1990).
- ²³K. J. Kim, B. N. Harmon, and D. W. Lynch, *Phys. Rev. B* **43**, 1948 (1991).
- ²⁴V. L. Moruzzi, A. R. Williams, and J. F. Janak, *Phys. Rev. B* **10**, 4856 (1974).
- ²⁵C. Muller, H. Wonn, W. Blau, P. Ziesche, and V. P. Krivitskii, *Phys. Status Solidi B* **95**, 215 (1979).
- ²⁶R. Eibler and A. Neckel, *J. Phys. F* **10**, 2179 (1980).
- ²⁷D. Knab and C. Koenig, *J. Phys. C* **2**, 465 (1990).
- ²⁸C. Colinet, A. Bessoud, and A. Pasturel, *J. Phys. Condens. Matter* **1**, 5837 (1989).
- ²⁹D. J. Peterman, R. Rosei, and D. W. Lynch, *Phys. Rev. B* **21**, 5505 (1980).
- ³⁰V. Ye. Yegorushkin, A. I. Kul'ment'yev, and P. E. Rubin, *Fiz. Metal. Metalloved.* **60**, 421 (1985).
- ³¹M. Mostoller, R. M. Nicklow, D. M. Zehner, S. C. Lui, J. M. Mundenar, and E. W. Plummer, *Phys. Rev. B* **40**, 2856 (1989).
- ³²J. A. Appelbaum and D. R. Hamann, in *Transition Metals*, edited by M. J. G. Lee, J. M. Perz, and E. Fawcett, IOP Conf. Proc. No. 39 (Institute of Physics and Physical Society, Bristol, 1977), p. 111; P. J. Feibelmann, J. A. Appelbaum, and D. R. Hamann, *Phys. Rev. B* **20**, 1433 (1979); B. N. Harmon, W. Weber, and D. R. Hamann, *ibid.* **25**, 1109 (1982).
- ³³G. L. Zhao, T. C. Leung, B. N. Harmon, M. Keil, M. Mullner, and W. Weber, *Phys. Rev. B* **40**, 7999 (1989).
- ³⁴C. M. Varma and W. Weber, *Phys. Rev. Lett.* **39**, 1094 (1977); *Phys. Rev. B* **19**, 6142 (1979).
- ³⁵W. Weber, in *Electronic Structure in Complex Systems*, edited by P. Phariseau and W. Temmerman, Series Vol. 113, of NATO-A.S.I. (Reidel, Holland, 1984), p. 345.
- ³⁶P. Moine, J. Allain, and B. Renker, *J. Phys. F* **14**, 2517 (1984).
- ³⁷H. Teitze, M. Müllner, and B. Renker, *J. Phys. C* **17**, L529 (1984).
- ³⁸G. M. Stocks, private communication.
- ³⁹P. C. Clapp, *Phys. Status Solidi B* **57**, 561 (1973); *Ferroelectrics* **16**, 89 (1977).